ACS SENSORS

pubs.acs.org/acssensors Article

UV Illumination as a Method to Improve the Performance of Gas Sensors Based on Graphene Field-Effect Transistors

Jaewoo Park,[†] Ranjana Rautela,[†] Natalia Alzate-Carvajal, Samantha Scarfe, Lukas Scarfe, Luc Alarie, Adina Luican-Mayer,* and Jean-Michel Ménard*

Cite This: https://doi.org/10.1021/acssensors.1c01783 Read Online

ACCESS | Metrics & More | Article Recommendations | Supporting Information

ABSTRACT: The ability to detect and recognize airborne chemical species is essential to enable applications in security, health, and environmental monitoring. Here, we report a sensing platform based on graphene field-effect transistor (GFET) devices combined with optical illumination for the detection of volatile compounds. We compare the change in resistance of GFET sensors upon exposure to analytes such as ethanol, dimethyl methylphosphonate (DMMP), and water vapors with and without the presence of a local illuminating ultraviolet (UV) light-emitting diode (LED). Our results show that UV illumination acts as a control knob for the electronic transport properties of graphene, increasing the device's response to ethanol, water, and DMMP, up to a factor of 54, and enabling ppb-level detection of DMMP at 800 ppb without chemical functionalization of the graphene layer. The sensing response can be optimized to reveal an analyte-specific interplay between the induced changes in carrier concentration and mobility of the GFET. These findings provide a pathway to enhancing the sensitivity of GFET sensors and a differentiation channel to improve their selectivity.

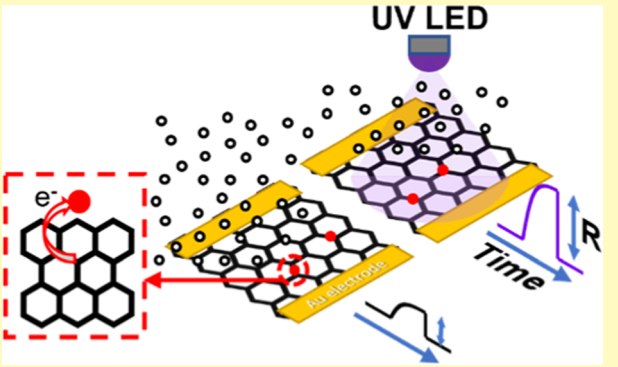

KEYWORDS: *graphene gas sensor, graphene field-effect transistor, UV, chemical warfare agent detection, sensing mechanism, 2D materials*

Gas sensing is an essential technique for monitoring environmental quality with applications in health, safety, and security. The success of this technology depends on the reliable detection and recognition of trace chemicals, which can enable disease detection through breath analysis or protect against security threats through chemical warfare agent detection.[1−3] In such applications, the analytes of interest are present in the ppb or ppt level[3,4] and mixed to other gases, requiring therefore both highly sensitive and selective sensing technologies.

Since their first demonstration in 2007,[5] gas sensors based on atomically thin (2D) materials have received a lot of interest. Due to their reduced dimensionality, surface-bound analytes have a larger impact on the material's macroscopic electrical properties, which significantly improves detection sensitivity.[6−9] Graphene-based devices are particularly promising in gas sensing applications due to their high electrical conductivity, low electrical noise, and chemical stability, among other properties. Sensors based on graphene and its derivatives were shown to be highly sensitive for the detection of analytes such as NO, NO_2, or NH_3.[10−16]

Previous work demonstrated that the sensitivity of graphene-based sensors can be modified by controlling the doping level[17−19] using different techniques such as surface functionalization,[19−21] the use of a field-effect transistor (FET) configuration,[22−24] and optical illumination of the graphene sensing layer.[25−28] Surface functionalization consists in modifying the surface properties of a material, generally via a thin deposition of molecules, to increase the material's degree of interaction with targeted analytes. Many types of functionalization techniques have led to selectively enhanced detection performances for gases such as NO_2 and NH_3.[19,20,29] For example, graphene can detect airborne SARS-CoV-2 when it is functionalized with spike protein antibodies.[30,31] This technique is very promising for many sensing applications, but it requires precise control of experimental parameters during the deposition process of the functionalization layer and does not provide any flexibility to account for sample-to-sample variations.[16] Other recent research based on a FET configuration shows improved sensitivity of graphene sensors when the doping level is adjusted via a bias voltage. Such a method was used to increase the device's sensitivity by optimizing the changes induced by bound analytes to

Received: August 19, 2021
Accepted: November 9, 2021

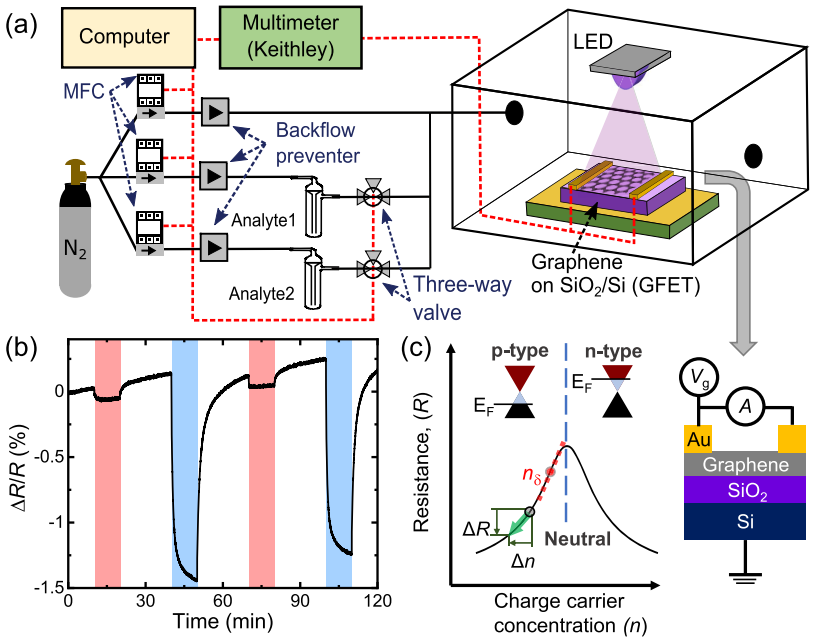

Figure 1. (a) Schematic of the experimental setup used to characterize graphene sensors. The resistance R of a graphene sheet is recorded as it is exposed to vapors of different analytes diluted in a N_2 carrier gas. An LED is placed above the graphene sensor, and it is used to homogeneously illuminate the sensing area. A back gate voltage (V_G) changing the doping level in graphene can be swept to extract electronic transport parameters. (b) Graphene sensor response when exposed to ethanol (red area) and water vapor (blue area) at a concentration of 2800 ppm without UV illumination. (c) (left) Schematic of the resistance of graphene R as a function of the charge carrier concentration n. A change in the carrier concentration, Δn, can be induced when graphene is exposed to analytes, resulting in a corresponding change in resistance ΔR. At the carrier density n_δ, located at the point of the highest slope, we find the maximum response ΔR for a given change in carrier concentration Δn. (right) We use a standard FET sensing configuration consisting of a graphene layer deposited on top of a Si/SiO_2 substrate. Two gold electrodes and an ammeter (A) are used to monitor the current flowing through graphene and extract its resistance, while a gate voltage (V_G) can be applied to modify the doping concentration of graphene.

graphene's macroscopic electrical properties.[17−19,24,32] However, the use of a gate voltage has two main drawbacks. First, this technique imposes restrictions on the device configuration, which relies on a doped substrate coated by a thin insulating layer. Then, only a relatively small change in doping concentration is generally induced by a low bias voltage (<30 V), while a higher bias voltage poses a risk of damaging the sensor by electrical arcing. To resolve this issue, UV illumination can also be used to change the doping level of graphene. Recent studies show that initially p-type doped graphene on a SiO_2 substrate experiences n-type doping under optical illumination of light at 365−405 nm wavelength.[25−27,33] This technique offers a promising alternative to the bias voltage configuration to tune the electrical properties of graphene, but more research is necessary for understanding underlying optically activated mechanisms and developing related applications in gas sensing, especially as it relates to improving detection selectivity.

Here, we address this need using a graphene chemiresistor under ultraviolet (UV) illumination to demonstrate enhanced sensitivity and a pathway toward selectivity. Our approach is fundamentally different from standard light-based detection techniques involving optical power and wavelength measurements, notably those related to spectroscopy. We rely instead on chemiresistive gas sensing, while the optical source is solely used to adjust the electrical properties of graphene, such as the doping level. We quantify the UV-enhanced detection response to vapors of ethanol, water, and dimethyl methylphosphonate (DMMP) and unveil, using a graphene field-effect transistor (GFET) configuration, an analyte-specific interplay between the changes in carrier concentration and mobility of the graphene. To our knowledge, this is the first time that graphene's electric properties are monitored while simultaneously conducting sensing experiments with and without optical illumination. This scheme allows us to explore the mechanisms leading to enhanced detection sensitivity and selectivity.

EXPERIMENTAL SECTION

Sensor Fabrication. The graphene film is obtained from commercially available graphene grown by chemical vapor deposition on a copper sheet, which is cut in square sections of 0.5 cm × 0.5 cm and covered with a 500 nm layer of poly(methyl methacrylate) (PMMA). To ensure proper transfer of the graphene film and efficient etching of the copper foil, the backside of the foil is exposed to an oxygen-based reactive ion etching. Subsequently, the sample is sunk in copper etchant and the floating PMMA/graphene film is transferred onto a Si/SiO_2 substrate (oxide thickness 285 nm). The PMMA layer covering the graphene is removed in two steps: first by cleaning the sample in an acetone bath at 50 °C for 1 h and second by thermal annealing for 1 h, and in some cases for 10 h, at 400 °C under an argon−hydrogen 5% atmosphere. Finally, two rectangular gold electrodes are thermally evaporated in a thermo/electron beam evaporator (Nexdep Series, Angstrom) using a shadow mask placed on top of the graphene surface. An illustration of our sensor geometry connected by gold wire bonds to a PCB mount is shown in Figure 1a. A picture of the device is included in the Supporting Information (Figure SI1).

GFET Sensor Testing. Experiments monitoring GFET characteristics in the presence of target analytes are carried out in a 250 mL dynamic gas flow chamber, as shown in Figure 1. Three mass flow controllers (MFCs) are connected to the chamber to supply gas throughout a single output. The ratio and flow rate of gas is controlled

https://doi.org/10.1021/acssensors.1c01783
ACS Sens. XXXX, XXX, XXX−XXX

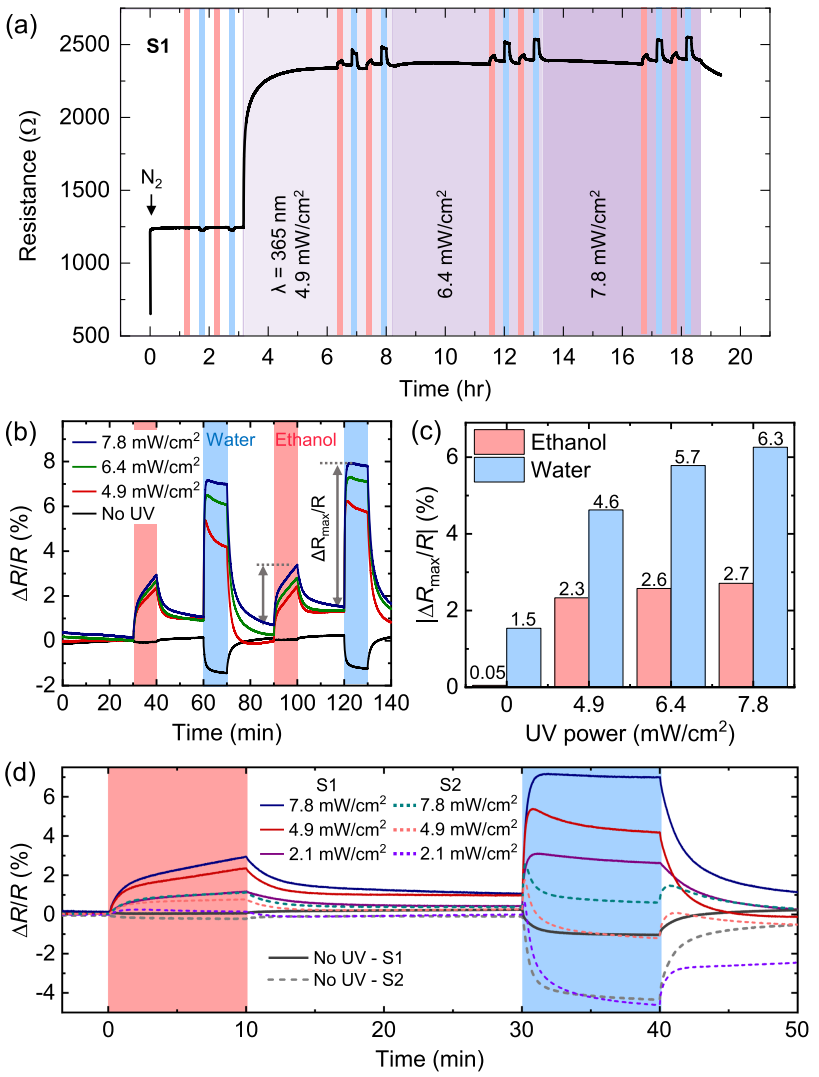

Figure 2. (a) Real-time monitoring of the resistance R of a graphene sensor, S1, in the dark (left region) and under increasing intensities of UV light at λ = 365 nm (right region with violet background). Data are collected when the device is under a pure N_2 atmosphere (white regions), exposed to 2800 ppm of diluted ethanol vapor (red regions), or exposed to 2800 ppm of diluted water vapor (blue regions). (b) Relative sensing responses are shown in % for comparison and (c) the corresponding peak-to-peak responses ($|\Delta R_{max}|/R$) are extracted for different intensities of optical illumination. (d) UV-assisted controllability of the sensing response to ethanol (2800 ppm) and water (2800 ppm) is demonstrated at different UV intensities with two graphene-based sensors prepared with different thermal annealing times (S1: 1 h and S2: 10 h).

by MFCs. Two lines are connected to a bubbler for carrying vapors to the chamber. The bubblers are kept at room temperature to accurately access a wider range of low gas concentrations. The electrical resistance of the graphene sheet is measured every 3 s from the linear I/V characteristic curve obtained by a multimeter (Keithley 2400) by keeping the voltage constant and recording the current. Commercial humidity, temperature, and ethanol detectors are also integrated inside our sensor chamber to ensure that environmental conditions are stable. An LED located ~3 cm above the sensing area allows homogeneous illumination of the device. The LEDs used in our experiments have wavelengths λ = 365, 405, or 850 nm and deliver an adjustable optical intensity between 0 and 7.8 mW/cm^2 over the 0.5 cm × 0.5 cm sensing area. Finally, all measurements are carried out at room temperature.

RESULTS AND DISCUSSION

Graphene devices are prepared and tested as described in the Experimental Section. Figure 1a shows a schematic of the experimental configuration that we use to investigate the sensor's response when exposed to vapors of ethanol (C_2H_5OH), water (H_2O), or dimethyl methylphosphonate (DMMP, $C_3H_9O_3P$) mixed with pure nitrogen (N_2) as carrier gas. At the start of each experiment, we purge the sensor chamber with N_2 until the graphene resistance reaches an equilibrium value under a stable and analyte-free environment. The sensing response to an analyte is then monitored as $\Delta R/R$, the ratio between the change in resistance of the GFET (ΔR) and its resistance in the absence of the analyte (R), as shown in Figure 2b. An LED with wavelength λ = 365 nm can be switched on to uniformly illuminate the entirety of the graphene sensing area.

Using this setup, we first characterize the graphene sensors' response in the absence of LED illumination, as shown in Figure 1b for ethanol and water vapor. Gas sensing experiments are conducted in a regime where the static resistance (or baseline) is constant. The sensing response depends on the nature of the analyte since the sensing mechanism involves molecule-specific charge transfer or local gating processes. In the GFET configuration, when a back gate

https://doi.org/10.1021/acssensors.1c01783
ACS Sens. XXXX, XXX, XXX−XXX

voltage (V_G) is swept to tune graphene's charge carrier concentration n, we monitor changes in the resistance as schematically represented in Figure 1c. These back gate measurements, performed before and during exposure to an analyte, reveal two key quantities: the charge carrier concentration n and charge carrier mobility μ of the graphene, both of which can be modified by the presence of analytes. The point of maximum R, corresponds to the Dirac point, separates the p-doped and n-doped regions as indicated in Figure 1c. In our experiment, ethanol acts as an electron acceptor taking free electrons from graphene and yielding a larger concentration of holes.[16] Our sensors are p-doped; therefore, we observe a decrease in resistance caused by an increase in hole concentration, as indicated by the direction of Δn in Figure 1c. Similarly, we observe a decrease in resistance when the sensors are exposed to water vapor, indicating that the water molecule is an electron acceptor, in agreement with previous work.[27] Furthermore, the larger signal observed for water vapor, in comparison to ethanol vapor at the same concentration, can be attributed to the strong polarity of the H_2O molecule.[34]

Next, we investigate the detection properties of graphene-based sensors under UV illumination. Figure 2a shows that UV illumination has an n-type doping effect resulting in an increase in the resistance of the p-type doped graphene sensor. This effect might be caused by optically induced desorption of p-type doping impurities, as discussed later in the paper. The resistance change also suggests that the device remains in the p-type region during the whole experiment since the resistance curve has no inflexion point indicative of a transition from a p-type to an n-type doping. Figure 2b shows the sensing response to water and ethanol vapors when the graphene layer is homogeneously illuminated with a UV LED (λ = 365 nm) at different optical intensities (including LED off for reference). When the LED is off, a negative change in resistance is consistently observed for both ethanol and water. Under UV illumination, the response is positive and significantly larger for both gases. As a general metric to determine the device sensitivity, which also applies when the response signal is not gradually increasing, we use the maximum signal change observed during a 10 min exposure to the analyte, $|\Delta R_{max}|/R$. As shown in Figure 2c, large UV intensities lead to an increase in sensitivity, by a factor up to 54 for ethanol and 4.2 for water. The overall shape of the time-dependent response of the sensor to an analyte is also dependent on optical illumination conditions. For example, when water vapor is introduced in the sensing chamber with the LED on, we observe a fast increase in $\Delta R/R$, followed by a gradual decrease. This dependence is distinctively different than a response gradually increasing or decreasing toward a saturation value, as we observed in the case of ethanol with and without LED illumination. These distinctive responses are shown in Figure 2d, comparing results obtained with two sensors successively exposed to ethanol (blue region) and water vapors (red region) under different UV intensities. The GFET sensors S1 and S2 are prepared with the same protocol and thermally annealed for 1 and 10 h, respectively. This step in the fabrication process of the GFET is used to remove residues on the surface of graphene, which have been known to affect the sensing properties.[16] Both sensors qualitatively behave similarly to the presence of ethanol vapor: they feature a gradual decrease in $\Delta R/R$ when the LED is off and a gradual increase in $\Delta R/R$ with LED on. Their respective response to water vapor is, however, noticeably different. Under UV illumination, S2 features a sharp increase in response followed by a sudden decrease. This behavior occurs within less than 20 s after releasing the water vapor in the sensing chamber, resulting in a distinctive peak in the time-dependent signal. This peak is also present in the signal collected with S1 under UV illumination, although less pronounced. We note that the sample S1 was used in two separate experiments to collect data displayed in Figure 2b,d.

To better understand the underlying mechanisms behind the influence of the UV illumination on the sensing properties, we performed measurements at different excitation wavelengths using three LEDs at 365, 405, and 850 nm while keeping a constant optical intensity of 6.4 mW/cm^2 on the graphene surface (see Figure SI2 for an overview). For these experiments, we use another graphene-based sensor, S3, fabricated with the same procedure as S2 (10 h thermal annealing time). In this test, we use DMMP as an analyte, which acts as a strong electron donor, inducing a positive change in resistance of the graphene sensor with a higher response signal in comparison to other analytes such as water and NH_3.[35] DMMP is used as a simulant for sarin gas in chemical warfare agent (CWA) detection research due to similarities in their chemical structures.[36] In Figure 3a, we show the sensing response of S3 exposed to DMMP vapor in the dark and under UV illumination with three different wavelengths.

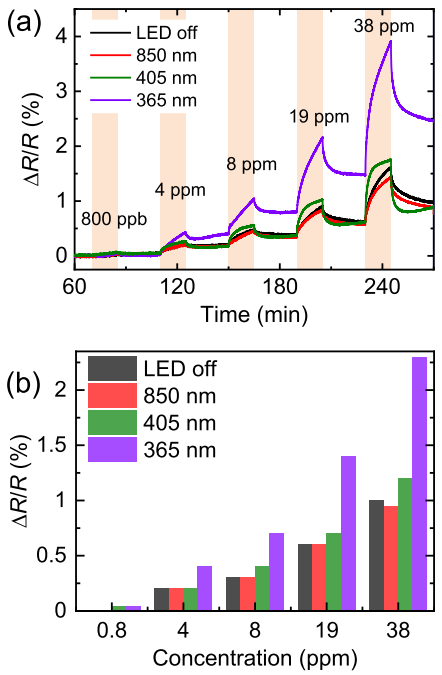

Figure 3. (a) Sensor's response in the presence of DMMP vapor at five concentrations under LED illumination with three different wavelengths (365, 405, and 850 nm at 6.4 mW/cm^2) and (b) peak-to-peak responses corresponding to the data in (a).

Unlike the case of ethanol and water vapors, the sensing response upon exposure to DMMP increases both without and with UV illumination. In Figure 3b, we show the maximum signal $|\Delta R_{max}|/R$ obtained from the data of Figure 3a. We find that the changes in sensitivity are wavelength-dependent. The effect of illuminating the GFET device with the wavelengths λ = 365 and 405 nm is to increase the maximum response signal by ∼50% and ∼10%, respectively. However, when

https://doi.org/10.1021/acssensors.1c01783
ACS Sens. XXXX, XXX, XXX−XXX

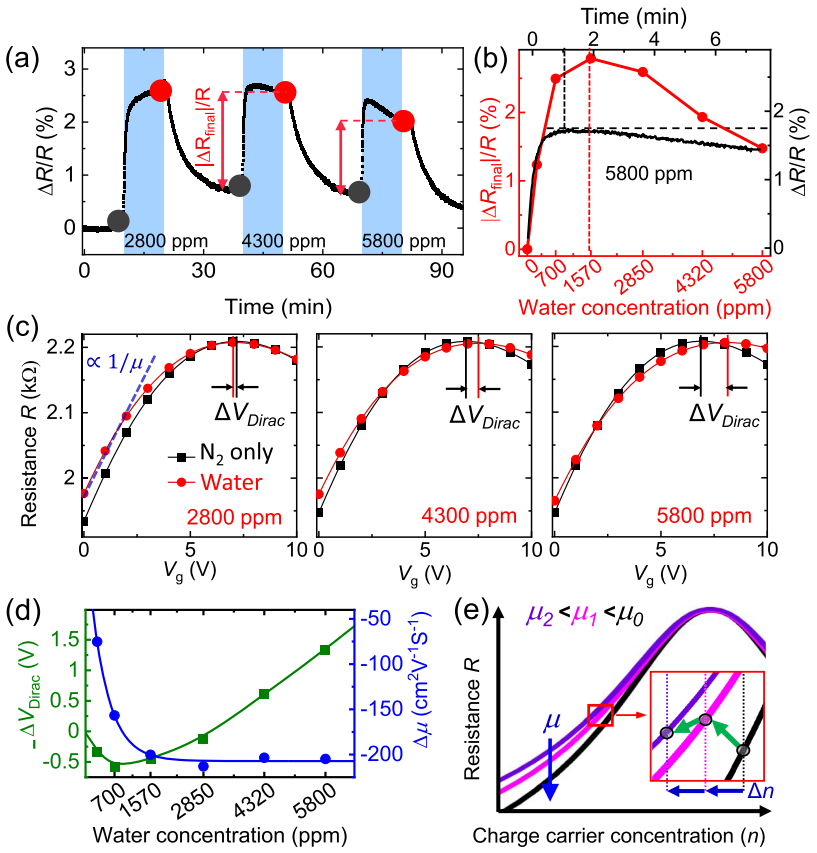

Figure 4. (a) GFET sensing response under UV illumination (λ = 365 nm, power = 1.7 mW/cm^2) at three different water vapor concentrations (2800, 4300, and 5800 ppm). (b) GFET resistance changes before and after exposure to water vapor for different concentrations. (c) GFET characteristics (resistance as a function of back gate voltage) measured before and during exposure to water vapor at the moments indicated by the dots in (a). (d) Change in V_G at Dirac point, ΔV_{Dirac}, and mobility change, $\Delta\mu$, upon exposure to different concentrations of water vapor. The line is a guide to the eye. (e) Schematic representation of how GFET's resistance can change upon varying the mobility and the charge carrier concentration.

illuminated with λ = 850 nm, the response shows no significant change compared to the case of no illumination. These wavelength-dependent measurements reveal a mechanism different than an interband optical injection of carriers in graphene since the material features a flat optical absorption in this spectral region that cannot justify a larger change at high photon energies (or short wavelengths).[37] Instead, another type of optical transition must be activated when the photon energy is above a certain level. This effect has been attributed to the excitation of impurities in the SiO_2/Si substrate.[25,27,33] More specifically, SiO_3−H defects in the 285 nm thick SiO_2 layer immediately underneath graphene can be excited by UV light resulting in free electrons gradually transferred to the graphene sheet.[25] Another interpretation involves an optical cleaning process allowing high-energy photons to effectively remove surface contaminants, such as H_2O and O_2 molecules, from the surface of graphene.[27,33]

The improved detection sensitivity upon UV illumination observed with all chemicals used in this work (ethanol, water, and DMMP) can be attributed to an optically induced change in the doping level of graphene.[27] More specifically, UV illumination shifts the graphene's carrier density toward a value corresponding to the maximum slope n, yielding a larger ΔR for a given Δn induced by an analyte. We note that in addition to changes in carrier concentration Δn, the sensing response can also be affected by changes in carrier mobility $\Delta\mu$ upon exposure to an analyte.[38−40] In our study, each of the three chemicals shows different changes in sensitivity upon UV illumination, suggesting that the changes in mobility and carrier concentration of GFETs are analyte-specific. Therefore, comparing signals from sensors in the dark and under optical illumination can be used to distinguish different compounds and enhance detection selectivity.

In addition to the relative increase in sensitivity, the qualitative dependence of the response as a function of exposure time to the analyte can be used as a differentiating feature among several analytes. We focus on the specific example of water vapor. As shown in Figure 2b,d, the signal can feature a distinctive peak in its time dependence, where we record a sharp increase in ΔR followed by a gradual decrease within tens of seconds. We investigate the origins of this specific signal by recording GFET characteristics in the presence of a varying back gate voltage V_G before and during exposure to water vapor. From these experiments, we extract two electrical properties of GFETs: the doping concentration n and carrier mobility μ. A GFET sensor S4 with a low carrier concentration is chosen so that the Dirac point can be reached within the available experimental range for V_G, allowing us to extract precise values for n and μ. Since the sensor's response to a given analyte concentration depends on the slope of the resistance as a function of carrier density, as shown in Figure 1c, S4 provides a sensing response weaker than those reported with devices S1−S3.

https://doi.org/10.1021/acssensors.1c01783
ACS Sens. XXXX, XXX, XXX−XXX

Immediately after releasing water vapors in the sensing chamber, the signal changes rapidly and this prevents us from collecting reliable resistance data as a function of V_G alone. As an alternate approach, we perform the measurement when the signal has reached a static value and repeat the process for different water vapor concentrations (Figure 4a) to reproduce experimental conditions at several data point of the time-dependent signal. We monitor the resistance dependence on V_G before releasing the analyte (black dots) and after 10 min of exposure when the sensor has reached a quasiequilibrium (red dots). This data provides detailed information about the changes in GFET parameters as a function of analyte concentration. Figure 4b shows a qualitative agreement between the time-dependent sensing response $|\Delta R|/R$ at 5800 ppm (black curve) and the sensing response measured after a ~10 min exposure to different water concentrations, $|\Delta R_{final}|/R$ (red curve). The difference in amplitudes can be attributed to a saturation effect after successive measurements at increasing concentrations, while the different positions of the peak signal (vertical dashed lines) can be effectively accounted for by the fast increase in water vapor concentration during the first minute following the release of the analyte inside the sensing chamber.

Figure 4c shows three examples of back gate measurements taken before (black curve) and during exposure to water vapor (red curve) corresponding to the signal shown in Figure 4a. Each set of back gate measurements ranging from 0 to 10 V is collected in only 0.76 s. This fast scan allows us to neglect any contribution from a potential drift in the static resistance (or baseline) on the measurements. We note that the Dirac point is resolved when applying a positive gate voltage, which confirms that our sensors are intrinsically (as-fabricated) p-doped. The monitored shift of the Dirac point before and after exposures, ΔV_{Dirac}, is displayed in Figure 4d (green line) and shows an overall increase at larger concentration. From the same data set, we use a numerical fit to extract the change in hole mobility $\Delta\mu$ (blue curve) and find a rapid change at low concentrations until 1570 ppm, where it reaches a plateau. As schematically represented in Figure 4e, a decrease in mobility when there is no change in n increases the resistance $\Delta R > 0$. This appears to be the dominant mechanism at low water vapor concentrations. However, above 2580 ppm, the change in mobility is negligible and the increase in hole density ($\Delta n > 0$) decreases the resistance $\Delta R < 0$. As a result, the peak signal observed when the sensor is exposed to a large enough concentration of water vapor (>1570 ppm for S4) can be explained by mobility and doping changing simultaneously but at different rates, depending on water vapor concentration (see inset of Figure 4e). The schematic of the graphene's resistance as a function of the carrier concentration is based on standard models.[41,42]

Another consequence of this dual interaction is the sign of ΔR induced by the presence of an analyte. Not only the target analyte may increase or decrease the carrier density $\pm \Delta n$ based on its specific interaction mechanism with graphene, but the sign of ΔR may also change under UV illumination as we observed for ethanol vapor.

The UV-induced changes in sensing properties are a robust phenomenon that is fully reversible within few hours and not invasive to the graphene sensing layer. Even after it has been stored for 1 year in air, the same sensor (S1) shows consistent results when exposed to ethanol and water, with and without UV illumination (Figure 5). For applications, we envision that the small discrepancies seen in Figure 5 can be improved by encapsulating the sensors.

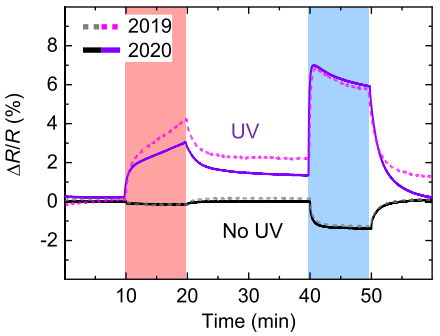

Figure 5. Sensor's response to ethanol and water vapor (both at 2800 ppm) of sensor S1 with and without UV illumination (λ = 365 nm, intensity of 6.4 mW/cm^2) repeated at 1 year interval.

CONCLUSIONS

In summary, we demonstrate a method to control the gas sensing response of GFET devices when the graphene surface is uniformly exposed to a low power of LED light. We investigate the sensing properties with three different analytes—ethanol, water, and DMMP vapors—and demonstrate an analyte-specific sensitivity enhancement factor up to 54, 4.2, and 2, respectively, which can be used to differentiate among target analytes. We also show that optical illumination can switch the sign of the detection signal and, more generally, the shape of the time-dependent response, hence providing additional selective information for analyte recognition. A wavelength-dependent study shows that the underlying mechanisms responsible for optically induced changes in the sensing response may involve optical interactions with the substrate or contaminants at the graphene surface. By investigating the specific response to water vapor with FET configuration of our sensor, we find that variations induced by changes in the carrier concentration n and mobility μ can affect the sign of the sensing response. The relative change rate of n and μ can cause nonmonotonic behavior of the time-dependent signal. In conclusion, UV illumination of a GFET sensor is an effective method to enhance gas detection sensitivity and to improve selectivity.

ASSOCIATED CONTENT

Supporting Information

The Supporting Information is available free of charge at https://pubs.acs.org/doi/10.1021/acssensors.1c01783.

Picture of a GFET gas sensing device; overall sensing test of a graphene sensor illuminated with different wavelengths of light; consistency of the signal amplitude to successive exposures to a constant DMMP vapor; and raw data corresponding to Figure 4a (PDF)

AUTHOR INFORMATION

Corresponding Authors

Adina Luican-Mayer − *Department of Physics, University of Ottawa, Ottawa, Ontario K1N 6N5, Canada;* orcid.org/0000-0001-9537-4600; Email: Luican-Mayer@uottawa.ca

Jean-Michel Ménard − *Department of Physics, University of Ottawa, Ottawa, Ontario K1N 6N5, Canada;* orcid.org/

https://doi.org/10.1021/acssensors.1c01783
ACS Sens. XXXX, XXX, XXX−XXX

0000-0002-6458-758X; Email: jean-michel.menard@uottawa.ca

Authors

Jaewoo Park − *Department of Physics, University of Ottawa, Ottawa, Ontario K1N 6N5, Canada*

Ranjana Rautela − *Department of Physics, University of Ottawa, Ottawa, Ontario K1N 6N5, Canada*

Natalia Alzate-Carvajal − *Department of Physics, University of Ottawa, Ottawa, Ontario K1N 6N5, Canada*

Samantha Scarfe − *Department of Physics, University of Ottawa, Ottawa, Ontario K1N 6N5, Canada*

Lukas Scarfe − *Department of Physics, University of Ottawa, Ottawa, Ontario K1N 6N5, Canada*

Luc Alarie − *Department of Physics, University of Ottawa, Ottawa, Ontario K1N 6N5, Canada*

Complete contact information is available at: https://pubs.acs.org/10.1021/acssensors.1c01783

Author Contributions

†J.P. and R.R. contributed equally.

Notes

The authors declare no competing financial interest.

■ ACKNOWLEDGMENTS

The authors acknowledge financial support from the Department of National Defense of Canada (DND-IDEaS; IDEaS-1-1A-CP-0122).

■ ABBREVIATIONS

GFET, graphene field-effect transistor; DMMP, dimethyl methylphosphonate; UV, ultraviolet; LED, light-emitting diode; CVD, chemical vapor deposition; MFC, mass flow controller; CWA, chemical warfare agent

■ REFERENCES

(1) Saalberg, Y.; Wolff, M. VOC Breath Biomarkers in Lung Cancer. *Clin. Chim. Acta* **2016**, *459*, 5−9.

(2) Voss, A.; Witt, K.; Kaschowitz, T.; Poitz, W.; Ebert, A.; Roser, P.; Bär, K. J. Detecting Cannabis Use on the Human Skin Surface via an Electronic Nose System. *Sensors* **2014**, *14*, No. 13256.

(3) Spencer, R. C. *Chemical and Biological Terrorism: Research and Development to Improve Civilian Medical Response*; National Academies Press, 2000; Vol. *46*.

(4) Blanchet, L.; Smolinska, A.; Baranska, A.; Tigchelaar, E.; Swertz, M.; Zhernakova, A.; Dallinga, J. W.; Wijmenga, C.; Van Schooten, F. J. Factors That Influence the Volatile Organic Compound Content in Human Breath. *J. Breath Res.* **2017**, *11*, No. 016013.

(5) Schedin, F.; Geim, A. K.; Morozov, S. V.; Hill, E. W.; Blake, P.; Katsnelson, M. I.; Novoselov, K. S. Detection of Individual Gas Molecules Adsorbed on Graphene. *Nat. Mater.* **2007**, *6*, 652−655.

(6) Varghese, S. S.; Lonkar, S.; Singh, K. K.; Swaminathan, S.; Abdala, A. Recent Advances in Graphene Based Gas Sensors. *Sens. Actuators, B* **2015**, *218*, 160−183.

(7) Yang, W.; Gan, L.; Li, H.; Zhai, T. Two-Dimensional Layered Nanomaterials for Gas-Sensing Applications. *Inorg. Chem. Front.* **2016**, *3*, 433−451.

(8) Mackin, C.; Fasoli, A.; Xue, M.; Lin, Y.; Adebiyi, A.; Bozano, L.; Palacios, T. Chemical Sensor Systems Based on 2D and Thin Film Materials. *2D Mater.* **2020**, *7*, No. 022002.

(9) Zhang, J.; Liu, X.; Neri, G.; Pinna, N. Nanostructured Materials for Room-Temperature Gas Sensors. *Adv. Mater.* **2016**, *28*, No. 1503825.

(10) Cagliani, A.; Mackenzie, D. M. A.; Tschammer, L. K.; Pizzocchero, F.; Almdal, K.; Bøggild, P. Large-Area Nanopatterned Graphene for Ultrasensitive Gas Sensing. *Nano Res.* **2014**, *7*, 743−754.

(11) Yavari, F.; Castillo, E.; Gullapalli, H.; Ajayan, P. M.; Koratkar, N. High Sensitivity Detection of NO 2 and NH 3 in Air Using Chemical Vapor Deposition Grown Graphene. *Appl. Phys. Lett.* **2012**, *100*, No. 203120.

(12) Fan, Y. Y.; Tu, H. L.; Pang, Y.; Wei, F.; Zhao, H.; Yang, Y.; Ren, T. L. Au-Decorated Porous Structure Graphene with Enhanced Sensing Performance for Low-Concentration NO2 Detection. *Rare Met.* **2020**, *39*, 651−658.

(13) Guo, L.; Li, T. Sub-Ppb and Ultra Selective Nitrogen Dioxide Sensor Based on Sulfur Doped Graphene. *Sens. Actuators, B* **2018**, *255*, 2258−2263.

(14) Ko, G.; Kim, H. Y.; Ahn, J.; Park, Y. M.; Lee, K. Y.; Kim, J. Graphene-Based Nitrogen Dioxide Gas Sensors. *Curr. Appl. Phys.* **2010**, *10*, 1002−1004.

(15) Cadore, A. R.; Mania, E.; Alencar, A. B.; Rezende, N. P.; de Oliveira, S.; Watanabe, K.; Taniguchi, T.; Chacham, H.; Campos, L. C.; Lacerda, R. G. Enhancing the Response of NH3 Graphene-Sensors by Using Devices with Different Graphene-Substrate Distances. *Sens. Actuators, B* **2018**, *266*, 438−446.

(16) Rautela, R.; Scarfe, S.; Guay, J. M.; Lazar, P.; Pykal, M.; Azimi, S.; Grenapin, C.; Boddison-Chouinard, J.; Halpin, A.; Wang, W.; Andrzejewski, L.; Plumadore, R.; Park, J.; Ménard, J. M.; Otyepka, M.; Luican-Mayer, A. Mechanistic Insight into the Limiting Factors of Graphene-Based Environmental Sensors. *ACS Appl. Mater. Interfaces* **2020**, *12*, 39764−39771.

(17) Bu, X.; Ma, F.; Wu, H.; Wu, Q.; Han, C.; Wang, X.; Li, X.; Liu, W. Highly Tunable Gas Sensing Performance of Graphene-Metal Contact by Gate Bias. *Mater. Lett.* **2020**, *275*, No. 128132.

(18) Lu, G.; Yu, K.; Ocola, L. E.; Chen, J. Ultrafast Room Temperature NH3 Sensing with Positively Gated Reduced Graphene Oxide Field-Effect Transistors. *Chem. Commun.* **2011**, *47*, 7761−7763.

(19) Solís-Fernández, P.; Okada, S.; Sato, T.; Tsuji, M.; Ago, H. Gate-Tunable Dirac Point of Molecular Doped Graphene. *ACS Nano* **2016**, *10*, 2930−2939.

(20) Alzate-Carvajal, N.; Luican-Mayer, A. Functionalized Graphene Surfaces for Selective Gas Sensing. *ACS Omega* **2020**, *34*, 21320−21329.

(21) Tang, X.; Debliquy, M.; Lahem, D.; Yan, Y.; Raskin, J. P. A Review on Functionalized Graphene Sensors for Detection of Ammonia. *Sensors* **2021**, *21*, No. 1443.

(22) Liu, Y.; Chang, J.; Lin, L. In *A Flexible Graphene FET Gas Sensor Using Polymer as Gate Dielectrics*, Proceedings of the IEEE International Conference on Micro Electro Mechanical Systems (MEMS), 2014.

(23) Łuszczek, M. Modelling of Graphene Field-Effect Transistor for Electronic Sensing Applications. *Electrotech. Rev.* **2015**, *1*, No. 94024.

(24) Singh, A. K.; Uddin, M. A.; Tolson, J. T.; Maire-Afeli, H.; Sbrockey, N.; Tompa, G. S.; Spencer, M. G.; Vogt, T.; Sudarshan, T. S.; Koley, G. Electrically Tunable Molecular Doping of Graphene. *Appl. Phys. Lett.* **2013**, *102*, No. 043101.

(25) Cao, G.; Liu, X.; Zhang, Y.; Liu, W.; Deng, M.; Chen, G.; Zhang, G.; Li, Q.; Beka, L. G.; Li, X.; Wang, X. Photoinduced Hysteresis of Graphene Field-Effect Transistors Due to Hydrogen-Complexed Defects in Silicon Dioxide. *ACS Appl. Mater. Interfaces* **2019**, *11*, 12170−12178.

(26) Kim, Y. D.; Bae, M. H.; Seo, J. T.; Kim, Y. S.; Kim, H.; Lee, J. H.; Ahn, J. R.; Lee, S. W.; Chun, S. H.; Park, Y. D. Focused-Laser-Enabled p-n Junctions in Graphene Field-Effect Transistors. *ACS Nano* **2013**, *7*, 5850−5857.

(27) Luo, Z.; Pinto, N. J.; Davila, Y.; Charlie Johnson, A. T. Controlled Doping of Graphene Using Ultraviolet Irradiation. *Appl. Phys. Lett.* **2012**, *100*, No. 253108.

(28) Ho, P. H.; Chen, C. H.; Shih, F. Y.; Chang, Y. R.; Li, S. S.; Wang, W. H.; Shih, M. C.; Chen, W. T.; Chiu, Y. P.; Li, M. K.; Shih, Y. S.; Chen, C. W. Precisely Controlled Ultrastrong Photoinduced

Doping at Graphene-Heterostructures Assisted by Trap-State-Mediated Charge Transfer. *Adv. Mater.* **2015**, *27*, No. 1503592.
(29) Georgakilas, V.; Otyepka, M.; Bourlinos, A. B.; Chandra, V.; Kim, N.; Kemp, K. C.; Hobza, P.; Zboril, R.; Kim, K. S. Functionalization of Graphene: Covalent and Non-Covalent Approaches, Derivatives and Applications. *Chem. Rev.* **2012**, *112*, 6156−6214.
(30) Afroj, S.; Britnell, L.; Hasan, T.; Andreeva, D. V.; Novoselov, K. S.; Karim, N. Graphene-Based Technologies for Tackling COVID-19 and Future Pandemics. *Adv. Funct. Mater.* **2021**, *17*, No. 2107407.
(31) Seo, G.; Lee, G.; Kim, M. J.; Baek, S. H.; Choi, M.; Ku, K. B.; Lee, C. S.; Jun, S.; Park, D.; Kim, H. G.; Kim, S. J.; Lee, J. O.; Kim, B. T.; Park, E. C.; Kim, S., Il. Correction: Rapid Detection of COVID-19 Causative Virus (SARS-CoV-2) in Human Nasopharyngeal Swab Specimens Using Field-Effect Transistor-Based Biosensor. *ACS Nano* **2020**, *14*, 12257−12258.
(32) Cao, G.; Liu, X.; Liu, W.; Li, Q.; Li, X.; Wang, X. Chemical Environment Dominated Fermi Level Pinning of a Graphene Gas Sensor. *Carbon* **2017**, *124*, 57−63.
(33) Yang, C. M.; Chen, T. C.; Yang, Y. C.; Hsiao, M. C.; Meyyappan, M.; Lai, C. S. Ultraviolet Illumination Effect on Monolayer Graphene-Based Resistive Sensor for Acetone Detection. *Vacuum* **2017**, *140*, 89−95.
(34) Smith, A. D.; Elgammal, K.; Niklaus, F.; Delin, A.; Fischer, A. C.; Vaziri, S.; Forsberg, F.; Råsander, M.; Hugosson, H.; Bergqvist, L.; Schröder, S.; Kataria, S.; Östling, M.; Lemme, M. C. Resistive Graphene Humidity Sensors with Rapid and Direct Electrical Readout. *Nanoscale* **2015**, *7*, 19099−19109.
(35) Novak, J. P.; Snow, E. S.; Houser, E. J.; Park, D.; Stepnowski, J. L.; McGill, R. A. Nerve Agent Detection Using Networks of Single-Walled Carbon Nanotubes. *Appl. Phys. Lett.* **2003**, *83*, No. 4026.
(36) Bartelt-Hunt, S. L.; Knappe, D. R. U.; Barlaz, M. A. A Review of Chemical Warfare Agent Simulants for the Study of Environmental Behavior. *Crit. Rev. Environ. Sci. Technol.* **2008**, *38*, 112−136.
(37) Li, W.; Cheng, G.; Liang, Y.; Tian, B.; Liang, X.; Peng, L.; Hight Walker, A. R.; Gundlach, D. J.; Nguyen, N. V. Broadband Optical Properties of Graphene by Spectroscopic Ellipsometry. *Carbon* **2016**, *99*, 348−353.
(38) Das Sarma, S.; Adam, S.; Hwang, E. H.; Rossi, E. Electronic Transport in Two-Dimensional Graphene. *Rev. Mod. Phys.* **2011**, *83*, No. 407.
(39) Orzechowska, S.; Mazurek, A.; Świslocka, R.; Lewandowski, W. Electronic Nose: Recent Developments in Gas Sensing and Molecular Mechanisms of Graphene Detection and Other Materials. *Materials* **2020**, *13*, No. 80.
(40) Li, H.; Han, X.; Childress, A. S.; Rao, A. M.; Koley, G. Investigation of Carrier Density and Mobility Variations in Graphene Caused by Surface Adsorbates. *Physica E* **2019**, *107*, 96−100.
(41) Kim, S.; Nah, J.; Jo, I.; Shahrjerdi, D.; Colombo, L.; Yao, Z.; Tutuc, E.; Banerjee, S. K. Realization of a High Mobility Dual-Gated Graphene Field-Effect Transistor with Al2O3 Dielectric. *Appl. Phys. Lett.* **2009**, *94*, No. 062107.
(42) Dorgan, V. E.; Bae, M. H.; Pop, E. Mobility and Saturation Velocity in Graphene on SiO2. *Appl. Phys. Lett.* **2010**, *97*, No. 082112.

https://doi.org/10.1021/acssensors.1c01783
ACS Sens. XXXX, XXX, XXX−XXX